Acta Cryst. (1989). B45, 467–473

A Structural Study of Phase Transitions in $[N(CH_3)_4]_2MnCl_4$

BY HIROYUKI MASHIYAMA AND NAOHIRO KOSHIJI†

Department of Physics, Faculty of Science, Yamaguchi University, Yamaguchi 753, Japan

(*Received* 30 *January* 1989; *accepted* 7 *June* 1989)

Abstract

The structures of the disordered phase (I), the commensurate modulated phases (III and IV) and the low-temperature phase (V) of bis(tetramethylammonium) tetrachloromanganate(II) were determined by single-crystal X-ray diffractometry at 293, 273, 261 and 168 K, respectively. Phase I: orthorhombic, *Pmcn*, $a = 9{\cdot}046$ (1), $b = 15{\cdot}669$ (3), $c = 12{\cdot}333$ (3) Å, $V = 1748{\cdot}1$ Å^3, $Z = 4$, $D_x = 1{\cdot}303$ Mg m^{-3}, $R = 0{\cdot}050$ for 918 independent reflections. The $MnCl_4$ tetrahedra are disordered and the mean structure is isomorphous with that of $[N(CH_3)_4]_2ZnCl_4$ at room temperature [Wiesner, Srivastava, Kennard, DiVaira & Lingafelter (1967). *Acta Cryst.* **23**, 565–574]. Phase III: monoclinic, $P2_1/c$, $a = 9{\cdot}041$ (2), $b = 15{\cdot}626$ (6), $c = 24{\cdot}661$ (6) Å, $\alpha = 89{\cdot}96$ (3)°, $V = 3484{\cdot}0$ Å^3, $Z = 8$, $D_x = 1{\cdot}316$ Mg m^{-3}, $R = 0{\cdot}053$ for 3718 independent reflections. The $MnCl_4$ tetrahedra alternately take one of the two configurations of phase I. Phase IV: monoclinic, $P2_1/n$, $a = 9{\cdot}037$ (2), $b = 15{\cdot}589$ (3), $c = 36{\cdot}973$ (11) Å, $\gamma = 90{\cdot}22$ (2)°, $V = 5208{\cdot}4$ Å^3, $Z = 12$, $D_x = 1{\cdot}320$ Mg m^{-3}, $R = 0{\cdot}066$ for 4856 independent reflections. The threefold superstructure is characterized by the alternate rotation of the $MnCl_4$ tetrahedra about an axis parallel to the c axis. The $N(CH_3)_4$ tetrahedra at the same height as $MnCl_4$ rotate in the same sense as $MnCl_4$. Phase V: monoclinic, $P2_1/c$, $a = 8{\cdot}977$ (3), $b = 15{\cdot}334$ (7), $c = 12{\cdot}216$ (6) Å, $\beta = 90{\cdot}16$ (3)°, $V = 1681{\cdot}5$ Å^3, $Z = 4$, $D_x = 1{\cdot}363$ Mg m^{-3}, $R = 0{\cdot}040$ for 2587 independent reflections. Each $MnCl_4$ and $N(CH_3)_4$ tetrahedron rotates about an axis parallel to the b axis, as well as about the c axis. The successive structural transformations are discussed in terms of the crystal structure.

Introduction

Bis(tetramethylammonium) tetrachloromanganate(II), $[N(CH_3)_4]_2MnCl_4$, belongs to the group of A_2BX_4-type crystals, the incommensurate phases of which have recently been studied (Sawada, Shiroishi, Yamamoto, Takashige & Matsuo, 1978; Shimizu, Abe, Yasuda, Fujimoto, Sawada & Shiroishi, 1979). With decreasing temperature, four phase transitions are found in $[N(CH_3)_4]_2MnCl_4$ at 292·1, 291·5, 266·5 and 172 K (Gesi & Ozawa, 1984). At room temperature, the crystal takes the normal structure with space group *Pmcn* (phase I), which has been shown to be a β-K_2SO_4-type structure and is isostructural with $[N(CH_3)_4]_2ZnCl_4$ (Wiesner, Srivastava, Kennard, DiVaira & Lingafelter, 1967; Morosin 1967). An incommensurate phase (II) appears in a narrow temperature range from 292·1 to 291·5 K with a modulation wavenumber $k_z \simeq 0{\cdot}483c_0^*$ (Mashiyama & Tanisaki, 1981), where c_0^* stands for the reciprocal-lattice parameter of phase I. In the temperature range 291·5–266·5 K, the commensurate phase (III) is characterized by the modulation wavenumber $k_z = \frac{1}{2}c_0^*$ and takes the monoclinic space group $P2_1/c11$. This is followed by another commensurate phase (IV) with $k_z = \frac{1}{3}c_0^*$ (space group $P112_1/n$). Below 172 K the crystal takes another normal structure, whose space group has been conjectured as $P12_1/c1$ (Gesi & Ozawa, 1984).

From the similarity of pressure *versus* temperature phase diagrams, it is widely considered that various tetramethylammonium tetrachlorometallic compounds can be arranged in a common reduced phase diagram (Shimizu, Abe, Kokubo, Yasuda & Fujimoto, 1980; Gesi & Ozawa, 1984). In the phase diagram $[N(CH_3)_4]_2MnCl_4$ is located at the lowest pressure situation. Further, phases IV and V are considered to be isostructural with phases IV and V of the zincate compound, respectively. However, no more-detailed structural study has been reported so far to the authors' knowledge.

In this work, we discuss the successive phase transitions of $[N(CH_3)_4]_2MnCl_4$ on the basis of the refined structures of all the commensurate phases. It is found that the constituent tetrahedral molecules are disordered in phase I. Therefore, the β-K_2SO_4-type structure (Wiesner *et al.*, 1967) is only an averaged one at room temperature. With decreasing temperature, the molecule occupies one of the two sites. Displacive modes combine with this orientational freedom and the lower-temperature phases are realized successively. The crystal symmetries are similar to those of $[N(CH_3)_4]_2ZnCl_4$ and in agreement with group-theoretical considerations (Tanisaki & Mashiyama, 1980).

† Present address: Department of Physics, Faculty of Science, Kyushu University, Fukuoka 812, Japan.

0108-7681/89/050467-07$03.00

Experimental

Single crystals of $[N(CH_3)_4]_2MnCl_4$ were grown by slow evaporation of an aqueous solution of a stoichiometric mixture of $N(CH_3)_4Cl$ and $MnCl_2$ at about 303 K. The crystals are light yellow in color, transparent and deliquescent. Spherical specimens with radii of about 0·2 mm were prepared and mounted on a four-circle diffractometer (Rigaku AFC-5 for phases I, III and V; Nonius CAD-4 for phase IV). Cold nitrogen gas was used to lower the temperature, which was controlled within 1 K. Graphite-monochromated Mo $K\alpha$ radiation, generated with a rotating anode (50 kV, 150 mA; AFC-5) or with a vacuum tube (55 kV, 32 mA; CAD-4), was employed. Lattice parameters were determined from 24 reflections (±2, ±8, ±1), (±4, ±2, ±5) and (±5, ±1, ±2) with $2\theta = 23$–$25°$. The intensities were measured by the θ–2θ scan method with a scan speed of $10° \text{ min}^{-1}$ or by ω scans with a scan speed of $3° \text{ min}^{-1}$ (phase IV only). The background was counted at both ends of each scan. Four standard reflections were monitored every 100–200 observations; no significant variation was detected.

Absorption, Lorentz and polarization corrections were made. Only strong reflections [$F_o \geq 5\sigma(F_o)$] were used for structural analysis. Block-diagonal least-squares calculations were performed with a program rewritten from the diagonal least-squares program in *UNICS* (Sakurai, 1967), where the value of $wR^2 = \sum(|F_o| - |F_c|)^2/\sum F_o^2$ was minimized ($w = 1$). Atomic scattering factors and anomalous-dispersion corrections were taken from *International Tables for X-ray Crystallography* (1974). All H atoms were neglected and calculations converged with anisotropic thermal parameters. The crystal data are summarized in Table 1, where R is defined by $R = \sum||F_c| - |F_o||/\sum|F_o|$.

Table 1. *Crystal data of* $[N(CH_3)_4]_2MnCl_4$

Monochromated Mo $K\alpha$ radiation was used.

	I	III	IV	V
Measurement temperature (K)	293	273	261	168
Crystal system	Orthorhombic	Monoclinic	Monoclinic	Monoclinic
Space group	*Pmcn*	$P2_1/c11$	$P112_1/n$	$P12_1/c1$
Z	4	8	12	4
a (Å)	9·046 (1)	9·041 (2)	9·037 (2)	8·977 (3)
b (Å)	15·669 (3)	15·626 (6)	15·589 (3)	15·334 (7)
c (Å)	12·333 (3)	24·661 (6)	36·973 (11)	12·216 (6)
Monoclinic angle (°)	-	$\alpha = 89·96$ (3)	$\gamma = 90·22$ (3)	$\beta = 90·16$ (3)
Scan method	2θ–θ	2θ θ	ω	2θ θ
$2\theta_{max}$ (°)	50	50	45	50
Index range	$0 \leq h \leq 10$	$0 \leq h \leq 10$	$-9 \leq h \leq 9$	$0 \leq h \leq 10$
	$0 \leq k \leq 18$	$0 \leq k \leq 18$	$0 \leq k \leq 16$	$0 \leq k \leq 18$
	$0 \leq l \leq 14$	$-29 \leq l \leq 29$	$0 \leq l \leq 39$	$-14 \leq l \leq 14$
No. of measured reflections	1806	6836	7304	3301
No. of significant reflections [$F > 5\sigma(F)$]	925	3718	4856	2587
Absorption coefficient (mm^{-1})	1·324	1·328	1·332	1·376
Crystal radius (mm)	0·175	0·180	0·181	0·182
Transmission factors	0·708–0·718	0·700–0·710	0·696–0·708	0·687–0·699
Final values of R	0·050	0·053	0·066	0·040

Structure refinements

Phase I (*Pmcn*, 293 K)

Starting from the parameters of $[N(CH_3)_4]_2ZnCl_4$ determined by Wiesner *et al.* (1967), least-squares calculations converged at $R = 0·065$ (displacive model), where seven reflections (002, 013, 021, 040, 111, 131, 200) were omitted from the final stage of the calculations because they seemed to be affected by secondary extinction. Although the positional parameters converged at reasonable positions, the mean values of the equivalent isotropic thermal parameters for Cl and C atoms were rather large; 9·06 and 18·21 Å^2, respectively.

Since disordering of the $ZnCl_4$ ion has been suggested in $[N(CH_3)_4]_2ZnCl_4$ (Hasebe, Mashiyama & Tanisaki, 1985), we considered another model where each Cl and C atom can occupy two positions with equal probability (split-atom method). From the symmetry of the crystal, we assumed that these two positions are related by the mirror symmetry ($\sigma_x|\frac{1}{2}00$) (disordered model). Starting from the results of the displacive model, split atoms were assumed firstly for Cl and secondly for C atoms. The calculations converged at $R = 0·050$ ($R = 0·057$ including the above seven reflections), $wR = 0·057$, $S = 1·83$, $(\Delta/\sigma)_{max} = 0·36$, $\Delta\rho_{max} = 0·20$ e Å^{-3}.*

The significance test proposed by Hamilton (1965) indicates that the disordered model is more probable than the displacive one with 99·5% significance level. The final atomic parameters at 293 K are listed in Table 2. Projections of the structure on the *bc* and *ab* planes are shown in Fig. 1. The mean structure is isostructural with $[N(CH_3)_4]_2ZnCl_4$. The pairs of the atomic positions of the disordered model are within the thermal ellipsoids of the displacive model.

The basic cell structure can be characterized by two pseudo-hexagonal networks of six-membered rings of $MnCl_4$ and $N(CH_3)_4$ tetrahedra at $z \simeq \frac{1}{4}$ and $\frac{3}{4}$. And another kind of $N(CH_3)_4$ ions (hereafter the first tetramethylammonium ion is denoted by TMA1 and the second by TMA2) are situated at the vacant centers of the rings between two networks. Two configurations of the tetrachloromanganate (TCM) tetrahedra can be reached by $\pm9°$ rotation from the mirror plane about an axis parallel to the c axis. TMA1 also rotates about the c axis but TMA2 rotates about the b axis as well as the c axis. Bond

* Lists of structure factors and anisotropic thermal parameters have been deposited with the British Library Document Supply Centre as Supplementary Publication No. SUP 52030 (30 pp.). Copies may be obtained through The Executive Secretary, International Union of Crystallography, 5 Abbey Square, Chester CH1 2HU, England.

Table 2. *Final atomic coordinates* ($\times 10^4$) *and equivalent isotropic thermal parameters* ($\times 10^2$) *for phase* I *at* 293 K *with e.s.d.'s in parentheses*

Only one of the two positions related by mirror symmetry is shown for each split atom. Fixed parameters are denoted by (*). Here B_{eq} is given by $\frac{4}{3}\sum B_{ij}\mathbf{a}_i.\mathbf{a}_j$.

	x	y	z	B_{eq}(Å^2)
Mn	2500 (*)	4074 (1)	2456 (1)	375 (3)
Cl(1)	2682 (7)	4064 (3)	566 (2)	695 (10)
Cl(2)	2854 (5)	5454 (2)	3167 (3)	716 (15)
Cl(3)	270 (4)	3537 (3)	3060 (4)	712 (12)
Cl(4)	4491 (5)	3227 (3)	3085 (4)	684 (11)
N(1)	2500 (*)	964 (5)	1494 (6)	459 (20)
N(2)	7500 (*)	3259 (5)	84 (6)	438 (21)
C(1)	2135 (36)	995 (13)	2641 (10)	1321 (90)
C(2)	2028 (27)	71 (10)	1121 (14)	1064 (96)
C(3)	1557 (25)	1630 (12)	949 (19)	1212 (74)
C(4)	4033 (21)	1138 (20)	1200 (21)	1460 (104)
C(5)	7702 (32)	2389 (9)	566 (15)	1243 (57)
C(6)	6868 (25)	3845 (13)	916 (15)	1196 (87)
C(7)	6649 (24)	3244 (15)	−903 (16)	1294 (73)
C(8)	9002 (16)	3566 (10)	−171 (17)	810 (57)

lengths and angles of each molecule are given in Table 3.

Phase III ($P2_1/c11$, 273 K)

The superstructure with double cell dimensions along the c axis can be constructed by alternate occupation of the disordered molecules. Taking the

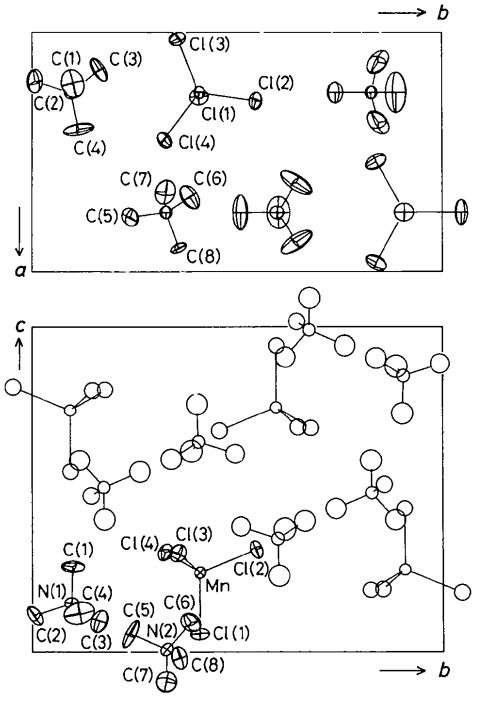

Fig. 1. Projection of the disordered structure at 293 K (phase I). In the *bc* plane, independent atoms are shown by thermal ellipsoids and other atoms by spheres. The radius represents the mean displacement estimated by the thermal parameter. In the *ab* plane, some of the split atoms are shown by the thermal ellipsoids. The tetrahedra of the displacive model are also drawn in the *ab* plane at the *n*-glide positions.

Table 3. *Bond lengths* (Å) *and bond angles* (°) *for phase* I *at* 293 K

Mn—Cl(1)	2·338 (4)	N(1)—C(1)	1·453 (17)	N(2)—C(5)	1·497 (19)
Mn—Cl(2)	2·354 (13)	N(1)—C(2)	1·534 (20)	N(2)—C(6)	1·491 (24)
Mn—Cl(3)	2·309 (13)	N(1)—C(3)	1·507 (24)	N(2)—C(7)	1·442 (23)
Mn—Cl(4)	2·369 (16)	N(1)—C(4)	1·460 (21)	N(2)—C(8)	1·475 (17)

Cl(1)—Mn—Cl(2)	111·6 (7)	Cl(1)—Mn—Cl(3)	112·4 (7)
Cl(1)—Mn—Cl(4)	105·6 (7)	Cl(2)—Mn—Cl(3)	109·5 (6)
Cl(2)—Mn—Cl(4)	106·8 (5)	Cl(3)—Mn—Cl(4)	110·7 (4)
C(1)—N(1)—C(2)	105·0 (11)	C(1)—N(1)—C(3)	106·4 (13)
C(1)—N(1)—C(4)	116·9 (14)	C(2)—N(1)—C(3)	109·9 (11)
C(2)—N(1)—C(4)	111·1 (11)	C(3)—N(1)—C(4)	107·3 (9)
C(5)—N(2)—C(6)	109·5 (8)	C(5)—N(2)—C(7)	112·7 (9)
C(5)—N(2)—C(8)	105·6 (13)	C(6)—N(2)—C(7)	112·8 (11)
C(6)—N(2)—C(8)	107·4 (9)	C(7)—N(2)—C(8)	108·4 (10)

symmetry of this phase into account, we assumed two independent models. In model *a*, two TCM tetrahedra at $z \simeq \frac{1}{8}$ and $\frac{3}{8}$ rotate in the same sense. On the other hand, they rotate in opposite sense in model *b*. Here the inversion center is located at the origin of the unit cell.

We firstly put all TCM and TMA ions at the mean positions of the disordered model and then allowed TCM ions to move in the least-squares calculations. After a few cycles of calculation, all TMA ions were also allowed to move so as to lower the R factors. Then the atomic parameters converged to the values corresponding to model *a*. We further refined the structure by considering the effect of the coexistence of two kinds of monoclinic domains. The R factor converged at $R = 0{\cdot}053$, $wR = 0{\cdot}062$, $S = 2{\cdot}8$, $(\Delta/\sigma)_{max} = 0{\cdot}84$ and $\Delta\rho_{max} = 0{\cdot}19$ e Å^{-3}. The best fitted domain ratio was 52·2:47·8.

The final atomic parameters are listed in Table 4. The structure projected on the *bc* plane is shown in Fig. 2. In a network at $z \simeq \frac{1}{8}, \frac{3}{8}, \frac{5}{8}$ and $\frac{7}{8}$, TCM and TMA1 tetrahedra rotate either clockwise or anticlockwise as viewed from the positive c axis. Hereafter, the former network is considered to be negative and the latter positive. Then the structure of phase III is a pile of −, +, + and − networks. The TMA2 between + and + or − and − networks rotates about the c axis in an opposite sense to the networks. Another kind of TMA2 sandwiched by + and − networks takes rather a neutral position similar to the displacive model of phase I. The bond lengths and angles given in Table 5 are in good agreement with those at 293 K.

Phase IV ($P112_1/n$, 261 K)

Three models of the superstructure with a threefold c axis can be constructed by alternative rotation of TCM. However, we started from the averaged structure of phase I. Firstly, TCM and then TMA ions were allowed to move. After a number of trial calculations, the refinement converged at $R = 0{\cdot}066$, where $wR = 0{\cdot}073$, $S = 4{\cdot}6$, $(\Delta/\sigma)_{max} = 0{\cdot}54$ and $\Delta\rho = 0{\cdot}33$ e Å^{-3} for 4856 independent reflections. The best estimated domain ratio was 64·8:35·2.

Table 4. *Final atomic coordinates* ($\times 10^4$) *and equivalent isotropic thermal parameters* ($\times 10^2$) *for phase* III *at* 273 K *with e.s.d.'s in parentheses*

	x	y	z	B_{eq}(Å^2)
Mn(*a*)	2543 (1)	4075 (1)	1222 (1)	370 (3)
Mn(*b*)	2705 (1)	933 (1)	3730 (1)	359 (3)
Cl(1*a*)	2659 (4)	4078 (3)	279 (1)	663 (9)
Cl(2*a*)	2894 (4)	5450 (2)	1593 (1)	727 (10)
Cl(3*a*)	228 (3)	3545 (3)	1510 (1)	699 (10)
Cl(4*a*)	4450 (4)	3209 (2)	1566 (1)	721 (10)
Cl(1*b*)	2679 (4)	939 (3)	2780 (1)	742 (10)
Cl(2*b*)	3034 (4)	−451 (2)	4085 (2)	705 (10)
Cl(3*b*)	447 (4)	1474 (3)	4053 (2)	779 (10)
Cl(4*b*)	4684 (4)	1799 (2)	4019 (2)	716 (9)
N(1*a*)	2655 (9)	936 (6)	737 (3)	484 (22)
N(1*b*)	2553 (8)	4033 (6)	3250 (3)	417 (20)
N(2*a*)	7555 (9)	3287 (5)	54 (3)	346 (19)
N(2*b*)	7618 (9)	1771 (6)	2528 (4)	512 (24)
C(1*a*)	2425 (22)	894 (12)	1364 (5)	1122 (61)
C(2*a*)	2228 (19)	107 (9)	484 (7)	981 (53)
C(3*a*)	1691 (21)	1604 (10)	472 (7)	1051 (60)
C(4*a*)	4210 (16)	1134 (14)	614 (7)	1162 (67)
C(1*b*)	2373 (20)	3925 (10)	3826 (4)	890 (50)
C(2*b*)	2106 (19)	4909 (8)	3071 (5)	847 (47)
C(3*b*)	1622 (20)	3362 (10)	2983 (7)	1053 (56)
C(4*b*)	4120 (16)	3879 (13)	3081 (7)	1103 (63)
C(5*a*)	7757 (18)	2398 (9)	286 (7)	1040 (53)
C(6*a*)	6686 (18)	3766 (12)	391 (8)	1416 (61)
C(7*a*)	6785 (21)	3185 (12)	−464 (6)	1436 (59)
C(8*a*)	9000 (15)	3632 (9)	−57 (7)	936 (52)
C(5*b*)	7566 (20)	2665 (9)	2715 (7)	1136 (58)
C(6*b*)	7441 (28)	1100 (11)	2980 (6)	1386 (84)
C(7*b*)	6410 (21)	1578 (13)	2190 (8)	1611 (69)
C(8*b*)	9070 (19)	1568 (11)	2303 (8)	1298 (66)

Table 5. *Bond lengths* (Å) *and bond angles* (°) *for phase* III *at* 273 K

Mn(*a*)—Cl(1*a*)	2·329 (3)	Mn(*b*)—Cl(1*b*)	2·344 (3)
Mn(*a*)—Cl(2*a*)	2·356 (25)	Mn(*b*)—Cl(2*b*)	2·352 (24)
Mn(*a*)—Cl(3*a*)	2·360 (8)	Mn(*b*)—Cl(3*b*)	2·349 (9)
Mn(*a*)—Cl(4*a*)	2·349 (15)	Mn(*b*)—Cl(4*b*)	2·354 (13)
N(1*a*)—C(1*a*)	1·562 (16)	N(1*b*)—C(1*b*)	1·439 (14)
N(1*a*)—C(2*a*)	1·490 (24)	N(1*b*)—C(2*b*)	1·494 (20)
N(1*a*)—C(3*a*)	1·508 (24)	N(1*b*)—C(3*b*)	1·497 (23)
N(1*a*)—C(4*a*)	1·472 (18)	N(1*b*)—C(4*b*)	1·496 (17)
N(2*a*)—C(5*a*)	1·514 (23)	N(2*b*)—C(5*b*)	1·472 (22)
N(2*a*)—C(6*a*)	1·367 (24)	N(2*b*)—C(6*b*)	1·538 (29)
N(2*a*)—C(7*a*)	1·466 (18)	N(2*b*)—C(7*b*)	1·407 (22)
N(2*a*)—C(8*a*)	1·439 (16)	N(2*b*)—C(8*b*)	1·460 (20)

Cl(1*a*)—Mn(*a*)—Cl(2*a*)	112·3 (14)	Cl(1*b*)—Mn(*b*)—Cl(2*b*)	112·1 (15)
Cl(1*a*)—Mn(*a*)—Cl(3*a*)	109·9 (6)	Cl(1*b*)—Mn(*b*)—Cl(3*b*)	109·2 (6)
Cl(1*a*)—Mn(*a*)—Cl(4*a*)	109·1 (9)	Cl(1*b*)—Mn(*b*)—Cl(4*b*)	107·9 (10)
Cl(2*a*)—Mn(*a*)—Cl(3*a*)	108·8 (4)	Cl(2*b*)—Mn(*b*)—Cl(3*b*)	108·4 (5)
Cl(2*a*)—Mn(*a*)—Cl(4*a*)	106·7 (3)	Cl(2*b*)—Mn(*b*)—Cl(4*b*)	108·7 (2)
Cl(3*a*)—Mn(*a*)—Cl(4*a*)	109·9 (7)	Cl(3*b*)—Mn(*b*)—Cl(4*b*)	110·5 (8)
C(1*a*)—N(1*a*)—C(2*a*)	110·1 (14)	C(1*b*)—N(1*b*)—C(2*b*)	111·5 (15)
C(1*a*)—N(1*a*)—C(3*a*)	112·4 (13)	C(1*b*)—N(1*b*)—C(3*b*)	106·8 (12)
C(1*a*)—N(1*a*)—C(4*a*)	109·9 (8)	C(1*b*)—N(1*b*)—C(4*b*)	111·3 (8)
C(2*a*)—N(1*a*)—C(3*a*)	105·7 (7)	C(2*b*)—N(1*b*)—C(3*b*)	111·1 (8)
C(2*a*)—N(1*a*)—C(4*a*)	110·1 (8)	C(2*b*)—N(1*b*)—C(4*b*)	108·7 (8)
C(3*a*)—N(1*a*)—C(4*a*)	108·5 (8)	C(3*b*)—N(1*b*)—C(4*b*)	107·3 (9)
C(5*a*)—N(2*a*)—C(6*a*)	110·0 (8)	C(5*b*)—N(2*b*)—C(6*b*)	114·6 (8)
C(5*a*)—N(2*a*)—C(7*a*)	106·7 (13)	C(5*b*)—N(2*b*)—C(7*b*)	111·4 (12)
C(5*a*)—N(2*a*)—C(8*a*)	107·8 (9)	C(5*b*)—N(2*b*)—C(8*b*)	110·8 (10)
C(6*a*)—N(2*a*)—C(7*a*)	108·6 (12)	C(6*b*)—N(2*b*)—C(7*b*)	101·6 (10)
C(6*a*)—N(2*a*)—C(8*a*)	115·7 (7)	C(6*b*)—N(2*b*)—C(8*b*)	102·8 (9)
C(7*a*)—N(2*a*)—C(8*a*)	107·7 (8)	C(7*b*)—N(2*b*)—C(8*b*)	115·2 (7)

The final atomic parameters are listed in Table 6. A projection of the structure along the *a* axis is shown in Fig. 3. The bond lengths and angles are given in Table 7. In phase IV, we can recognize the correlated arrangement between TCM and TMA1 in a network again; in each layer perpendicular to the *c* axis TMA1 tetrahedra rotate about the *c* axis in the same sense as TCM tetrahedra, and the networks are

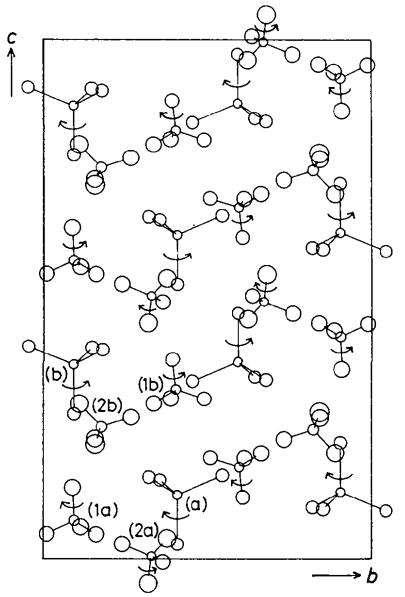

Fig. 2. Projection of the twofold commensurate structure at 273 K (phase III) along the *a* axis. The rotations of TCM and TMA1 about the *c* axis are indicated by arrows.

Table 6. *Final atomic coordinates* ($\times 10^4$) *and equivalent isotropic thermal parameters* ($\times 10^2$) *for phase* IV *at* 261 K *with e.s.d.'s in parentheses*

	x	y	z	B_{eq}(Å^2)
Mn(*a*)	2526 (2)	4088 (1)	816 (1)	324 (4)
Mn(*b*)	2794 (2)	4092 (1)	4157 (1)	328 (4)
Mn(*c*)	2256 (2)	4021 (1)	7489 (1)	338 (4)
Cl(1*a*)	2739 (4)	4061 (3)	184 (1)	609 (12)
Cl(2*a*)	2847 (5)	5477 (3)	1054 (1)	632 (12)
Cl(3*a*)	181 (4)	3555 (3)	995 (1)	651 (13)
Cl(4*a*)	4401 (4)	3230 (3)	1065 (1)	619 (11)
Cl(1*b*)	2604 (5)	4110 (3)	3523 (1)	629 (12)
Cl(2*b*)	3194 (5)	5482 (3)	4384 (1)	603 (12)
Cl(3*b*)	569 (4)	3567 (3)	4406 (1)	643 (12)
Cl(4*b*)	4810 (4)	3197 (3)	4323 (1)	613 (11)
Cl(1*c*)	2152 (5)	4070 (3)	6855 (1)	649 (12)
Cl(2*c*)	1890 (5)	5380 (3)	7761 (1)	633 (12)
Cl(3*c*)	371 (5)	3120 (3)	7695 (1)	670 (12)
Cl(4*c*)	4578 (4)	3491 (3)	7666 (1)	644 (12)
N(1*a*)	2749 (10)	954 (8)	496 (3)	426 (30)
N(1*b*)	2564 (10)	989 (6)	3828 (2)	273 (23)
N(1*c*)	2316 (12)	882 (9)	7161 (3)	548 (35)
N(2*a*)	7572 (10)	3241 (7)	35 (3)	370 (28)
N(2*b*)	7631 (11)	3263 (7)	3343 (3)	408 (29)
N(2*c*)	7258 (11)	3264 (7)	6693 (3)	420 (29)
C(1*a*)	2372 (23)	907 (21)	896 (5)	1167 (93)
C(2*a*)	2331 (20)	88 (12)	357 (5)	799 (56)
C(3*a*)	1789 (22)	1608 (12)	303 (6)	908 (65)
C(4*a*)	4370 (18)	1042 (15)	429 (7)	941 (73)
C(1*b*)	2487 (27)	1037 (14)	4228 (5)	951 (74)
C(2*b*)	2013 (21)	130 (12)	3711 (5)	810 (57)
C(3*b*)	1541 (27)	1559 (19)	3670 (7)	1411 (94)
C(4*b*)	4062 (18)	1165 (15)	3711 (5)	858 (65)
C(1*c*)	2552 (25)	996 (13)	7565 (4)	965 (66)
C(2*c*)	2766 (23)	33 (11)	7005 (6)	798 (63)
C(3*c*)	756 (18)	1129 (20)	7082 (6)	1218 (89)
C(4*c*)	3216 (21)	1627 (11)	6989 (4)	683 (53)
C(5*a*)	7868 (25)	2400 (14)	186 (7)	1045 (77)
C(6*a*)	6854 (20)	3862 (14)	323 (4)	882 (58)
C(7*a*)	6478 (21)	3166 (14)	−260 (5)	1004 (60)
C(8*a*)	9022 (18)	3650 (13)	−65 (6)	838 (65)
C(5*b*)	7490 (21)	2366 (10)	3439 (6)	853 (61)
C(6*b*)	8622 (32)	3661 (21)	3564 (8)	2183 (148)
C(7*b*)	6200 (21)	3616 (17)	3307 (9)	1476 (117)
C(8*b*)	8135 (36)	3245 (17)	2967 (6)	1762 (103)
C(5*c*)	7282 (23)	2294 (10)	6826 (6)	960 (61)
C(6*c*)	7885 (27)	3824 (13)	6954 (6)	1048 (114)
C(7*c*)	5775 (17)	3508 (10)	6585 (5)	711 (63)
C(8*c*)	8291 (23)	3438 (15)	6400 (6)	1343 (77)

stacked in −, +, −, −, + and − senses in the threefold cell. TMA2 tetrahedra at $z \simeq 0$ and $\frac{1}{2}$ rotate about the c axis in opposite sense to the networks, as in phase III. C atoms of other TMA2 ions sandwiched by the two networks of opposite sense take rather large thermal parameters, which may indicate that the TMA2 structure is disordered. However, no residual peak was visible in the difference Fourier synthesis.

Phase V ($P12_1/c1$, 168 K)

Space group $P12_1/c1$ was confirmed by extinction rules. The normal structure of phase V was analyzed by means of least-squares calculations from a set of starting parameters of the displacive model at 293 K. A few cycles of calculations converged successfully at $R = 0{\cdot}040$, $wR = 0{\cdot}050$, $S = 1{\cdot}8$, $(\Delta/\sigma)_{max} = 0{\cdot}32$ and $\Delta\rho = 0{\cdot}26$ e Å^{-3} with the domain ratio of 64·8:35·2 for 2580 independent reflections. The final atomic parameters are listed in Table 8. The bond lengths and angles are given in Table 9. Projections of the structure along the a and b axes are shown in Fig. 4. Each molecule in the unit cell rotates in a same sense about the b axis, which is related to a newly condensed mode to realize the monoclinic phase. Moreover, two TCM ions in a layered network rotate in opposite senses about the c axis. TMA1 tetrahedra also rotate in accordance with TCM.

Discussion

We have analyzed the crystal structures of $[N(CH_3)_4]_2MnCl_4$ (TMA–TCM). In the disordered phase (I), a TCM tetrahedron as well as a TMA tetrahedron occupy two sites related by mirror symmetry with equal probability, similar to the situation in $[N(CH_3)_4]_2ZnCl_4$ (Hasebe *et al.*, 1985; Hasebe, Mashiyama, Koshiji & Tanisaki, 1987).

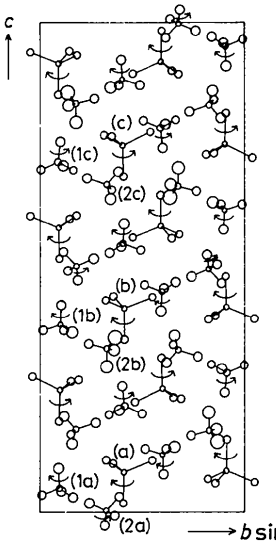

Fig. 3. Projection of the threefold commensurate structure at 261 K (phase IV) along the a axis. The rotations of TCM and TMA1 about the c axis are indicated by arrows.

Table 7. *Bond lengths* (Å) *and bond angles* (°) *for phase* IV *at* 261 K

	Type *a*	Type *b*	Type *c*
Mn—Cl(1)	2·345 (4)	2·349 (4)	2·345 (4)
Mn—Cl(2)	2·356 (9)	2·350 (11)	2·370 (10)
Mn—Cl(3)	2·368 (23)	2·356 (22)	2·332 (32)
Mn—Cl(4)	2·351 (30)	2·381 (3)	2·352 (23)
N(1)—C(1)	1·521 (21)	1·485 (21)	1·517 (20)
N(1)—C(2)	1·494 (24)	1·490 (25)	1·502 (25)
N(1)—C(3)	1·520 (29)	1·412 (34)	1·492 (24)
N(1)—C(4)	1·491 (20)	1·447 (21)	1·553 (29)
N(2)—C(5)	1·451 (25)	1·448 (19)	1·591 (20)
N(2)—C(6)	1·545 (22)	1·361 (33)	1·420 (25)
N(2)—C(7)	1·478 (21)	1·413 (25)	1·451 (20)
N(2)—C(8)	1·503 (22)	1·464 (26)	1·453 (25)
Cl(1)—Mn—Cl(2)	112·3 (2)	110·8 (1)	112·9 (2)
Cl(1)—Mn—Cl(3)	110·3 (2)	109·4 (2)	108·5 (3)
Cl(1)—Mn—Cl(4)	108·7 (4)	108·7 (2)	109·0 (2)
Cl(2)—Mn—Cl(3)	108·9 (14)	108·0 (13)	107·2 (9)
Cl(2)—Mn—Cl(4)	106·9 (9)	109·5 (10)	108·9 (13)
Cl(3)—Mn—Cl(4)	109·7 (4)	110·5 (4)	110·3 (5)
C(1)—N(1)—C(2)	103·7 (8)	108·6 (6)	116·3 (7)
C(1)—N(1)—C(3)	111·2 (10)	110·5 (10)	107·2 (9)
C(1)—N(1)—C(4)	112·7 (8)	109·4 (10)	104·1 (9)
C(2)—N(1)—C(3)	107·6 (9)	103·2 (12)	114·3 (16)
C(2)—N(1)—C(4)	105·7 (17)	113·2 (15)	111·0 (10)
C(3)—N(1)—C(4)	115·1 (11)	111·8 (10)	102·6 (12)
C(5)—N(2)—C(6)	111·7 (4)	110·4 (9)	111·5 (6)
C(5)—N(2)—C(7)	109·8 (9)	108·8 (13)	110·6 (12)
C(5)—N(2)—C(8)	108·4 (13)	104·0 (5)	113·4 (10)
C(6)—N(2)—C(7)	108·5 (11)	118·7 (8)	113·1 (9)
C(6)—N(2)—C(8)	102·9 (7)	112·0 (16)	97·9 (11)
C(7)—N(2)—C(8)	115·5 (4)	101·7 (12)	109·9 (7)

Table 8. *Final atomic coordinates* ($\times 10^4$) *and equivalent isotropic thermal parameters* ($\times 10^2$) *for phase* V *at* 168 K *with e.s.d.'s in parentheses*

	x	y	z	B_{eq}(Å^2)
Mn	2252 (1)	4054 (1)	2469 (1)	157 (1)
Cl(1)	2732 (2)	4073 (1)	573 (1)	236 (3)
Cl(2)	1875 (2)	5462 (1)	3187 (1)	298 (4)
Cl(3)	91 (2)	3217 (1)	2844 (1)	264 (4)
Cl(4)	4360 (2)	3435 (1)	3316 (1)	329 (3)
N(1)	2641 (6)	972 (3)	1496 (3)	205 (10)
N(2)	7520 (5)	3295 (3)	36 (4)	186 (10)
C(1)	2208 (9)	1030 (4)	2682 (4)	350 (16)
C(2)	2462 (12)	46 (4)	1115 (6)	466 (23)
C(3)	1635 (9)	1557 (5)	815 (6)	393 (18)
C(4)	4205 (9)	1250 (7)	1344 (7)	599 (27)
C(5)	7673 (9)	2345 (4)	336 (6)	337 (16)
C(6)	6806 (8)	3783 (5)	964 (6)	358 (17)
C(7)	6537 (9)	3380 (5)	−959 (5)	383 (16)
C(8)	9018 (7)	3650 (4)	−203 (6)	292 (17)

Table 9. *Bond lengths* (Å) *and bond angles* (°) *for phase* V *at* 168 K

Mn—Cl(1)	2·358 (15)	N(1)—C(1)	1·503 (15)	N(2)—C(5)	1·509 (7)
Mn—Cl(2)	2·356 (5)	N(1)—C(2)	1·504 (8)	N(2)—C(6)	1·504 (18)
Mn—Cl(3)	2·372 (13)	N(1)—C(3)	1·519 (19)	N(2)—C(7)	1·507 (26)
Mn—Cl(4)	2·353 (28)	N(1)—C(4)	1·480 (11)	N(2)—C(8)	1·481 (12)

Cl(1)—Mn—Cl(2)	112·4 (3)	Cl(1)—Mn—Cl(3)	110·4 (15)
Cl(1)—Mn—Cl(4)	106·7 (13)	Cl(2)—Mn—Cl(3)	107·8 (8)
Cl(2)—Mn—Cl(4)	108·8 (7)	Cl(3)—Mn—Cl(4)	110·7 (3)
C(1)—N(1)—C(2)	109·0 (3)	C(1)—N(1)—C(3)	109·8 (9)
C(1)—N(1)—C(4)	110·6 (17)	C(2)—N(1)—C(3)	109·0 (9)
C(2)—N(1)—C(4)	109·5 (8)	C(3)—N(1)—C(4)	108·9 (8)
C(5)—N(2)—C(6)	109·7 (4)	C(5)—N(2)—C(7)	109·4 (3)
C(5)—N(2)—C(8)	108·7 (5)	C(6)—N(2)—C(7)	108·5 (5)
C(6)—N(2)—C(8)	110·8 (13)	C(7)—N(2)—C(8)	109·8 (11)

On passing through the narrow temperature range of the incommensurate phase, the tetrahedra are ordered and the pseudo-hexagonal network changes its rotational sense alternately in phase III. In the unit cell viewed in the *ca* plane, we can note two chains along the *c* axis at $x \simeq \frac{1}{4}$ and $\frac{3}{4}$. The chains are seen to be modulated sinusoidally, and the phases of the modulation of the two chains are in phase for model *a*. Therefore the molecules are packed more uniformly than in model *b*, where the two modulations are out of phase.

In phase IV, the modulations along the *c* axis are also in phase with each other, and both TCM and TMA1 tetrahedra in the network rotate in the same sense. The rotation angles of the tetrahedra and the displacement of their centers of mass can be fitted to the relation

$$A_0 + A_1\cos(2\pi z) + B_1\sin(2\pi z). \qquad (1)$$

Fig. 5 shows the fitted relation. Here the rotation angles about the *b* and *c* axes are estimated from the positions of Cl(1) or C(1) and Cl(2) or C(2), respectively. In Fig. 5(*a*), the rotation angles of the tetrahedra about the *c* axis are nearly equal to those of phase I (indicated by broken horizontal lines). Therefore the modulation pattern of the rotation about the *c* axis is rectangular rather than sinusoidal. On the other hand, the displacement pattern of the centers of mass of tetrahedra along the *a* axis is sinusoidal. These results are in agreement with the partially disordered model of phase I in that the tetrahedra are only orientationally disordered and the centers of mass are located on the mirror plane (*i.e.* split atoms are assumed only for Cl and C).

Although phase IV is different from phase III in its modulation period and amplitudes, the basic features of these phases are very similar. According to group-theoretical considerations, phases III and IV are induced from phase I by condensation of a Z_2 mode at $k_z = \frac{1}{2}c_0^*$ and a Λ_2 mode at $\frac{1}{3}c_0^*$, respectively (Tanisaki & Mashiyama, 1980). These modes are connected by the compatibility relation. The monoclinic systems are induced by couplings between the primary-order parameter and the strain component. Since these couplings are higher-order ones, the modulations resemble each other.

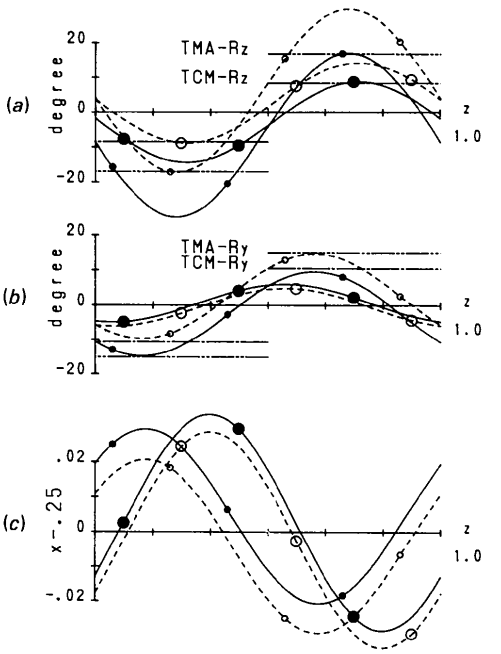

Fig. 5. The modulation pattern at 261 K (phase IV). The rotation angles of TCM (large circles) and TMA1 (small circles) are shown in (*a*) about the *c* axis and in (*b*) about the *b* axis. The displacements of their centers of mass along the *a* axis are shown in (*c*). The open circles are related to the closed ones by $\frac{1}{2} - x, \frac{1}{2} - y, \frac{1}{2} + z$. Sinusoidal curves are fitted to equation (1). The broken horizontal lines in (*a*) and (*b*) indicate the rotation angle of phase I (disordered model).

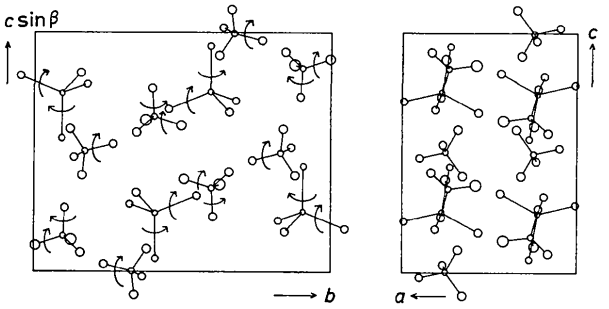

Fig. 4. Projections of the structure at 168 K (phase V) along the *a* and *b* axes. The rotations of the tetrahedra about the *b* and *c* axes are indicated by arrows.

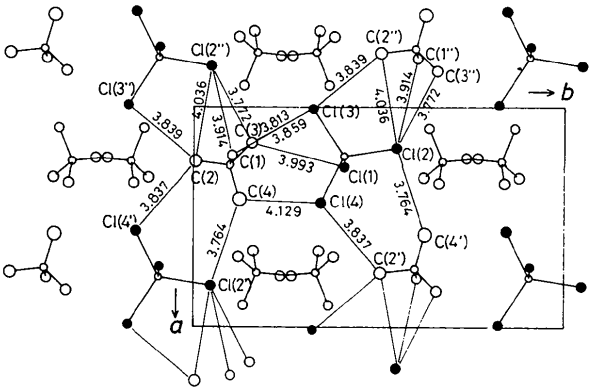

Fig. 6. Projection of the network system of TCA and TMA1 around $z \simeq \frac{1}{4}$ in phase V. Atomic distances (Å) shorter than 4·2 Å are shown.

As mentioned in the previous section, the condensation of the rotational mode about the b axis induces phase V, which belongs to Γ_5 representation of phase I. The modulation patterns in a network at $z \simeq \frac{1}{4}$ are shown in Fig. 6, where the neighboring atoms are linked by lines. The opposite rotations of tetrahedra in two chains along the a axis can be interpreted as follows: $MnCl_4(x \simeq \frac{1}{4}, y \simeq 0{\cdot}4)$ rotates clockwise about the b axis and counterclockwise about the c axis. Then the C(3)–Cl(3) distance becomes shorter than the C(4)—Cl(4) distance. If the shorter distance is preferable for C—H—Cl bonding, then $N(CH_3)_4(x \simeq \frac{1}{4}, y \simeq 0{\cdot}1)$ rotates clockwise about the c axis. From Fig. 6, the C—H—Cl bond length is 3·76–3·84 Å. This bonding may be important for realizing the low-temperature structure.

The authors are grateful to Professor A. Okazaki and Dr Machida for the use of the four-circle diffractometer (Nonius CAD-4) and for invaluable help in the data collection at the Center of Advanced Instrumental Analysis, Kyushu University, Japan.

References

GESI, K. & OZAWA, K. (1984). *J. Phys. Soc. Jpn*, **53**, 627–634.
HAMILTON, W. C. (1965). *Acta Cryst.* **18**, 502–510.
HASEBE, K., MASHIYAMA, H., KOSHIJI, N. & TANISAKI, S. (1987). *J. Phys. Soc. Jpn*, **56**, 3543–3552.
HASEBE, K., MASHIYAMA, H. & TANISAKI, S. (1985). *Jpn J. Appl. Phys.* **24**, 802–804.
International Tables for X-ray Crystallography (1974). Vol. IV. Birmingham: Kynoch Press. (Present distributor Kluwer Academic Publishers, Dordrecht.)
MASHIYAMA, H. & TANISAKI, S. (1981). *J. Phys. Soc. Jpn*, **50**, 1413–1414.
MOROSIN, B. (1967). Quoted in Wiesner *et al.* (1967), p. 573.
SAKURAI, T. (1967). Editor. *Universal Crystallographic Computation Program System*. The Crystallographic Society of Japan, Tokyo, Japan.
SAWADA, S., SHIROISHI, Y., YAMAMOTO, A., TAKASHIGE, M. & MATSUO, M. (1978). *Phys. Lett. A*, **67**, 56–58.
SHIMIZU, H., ABE, N., KOKUBO, N., YASUDA, N. & FUJIMOTO, S. (1980). *Solid State Commun.* **34**, 363–368.
SHIMIZU, H., ABE, N., YASUDA, N., FUJIMOTO, S., SAWADA, S. & SHIROISHI, Y. (1979). *Jpn J. Appl. Phys.* **18**, 857.
TANISAKI, S. & MASHIYAMA, H. (1980). *J. Phys. Soc. Jpn*, **48**, 339–340.
WIESNER, J. R., SRIVASTAVA, R. C., KENNARD, C. H. L., DIVAIRA, M. & LINGAFELTER, E. C. (1967). *Acta Cryst.* **23**, 565–574.

Acta Cryst. (1989). B**45**, 473–482

Crystal Structures of Polynuclear Aromatic Hydrocarbons. Classification, Rationalization and Prediction from Molecular Structure

BY GAUTAM R. DESIRAJU

School of Chemistry, University of Hyderabad, PO Central University, Hyderabad 500 134, *India*

AND A. GAVEZZOTTI

Dipartimento di Chimica Fisica ed Elettrochimica e Centro CNR, Universita di Milano, via Golgi 19, 20133 *Milano, Italy*

(*Received* 4 *October* 1988; *accepted* 21 *March* 1989)

Abstract

Polynuclear aromatic hydrocarbons crystallize in four basic structure types which may be clearly differentiated by energetic and geometrical criteria. The major motifs in these four prototypes are the stack, or layer, and the glide, or herringbone. A study of 32 representative hydrocarbons shows that the adoption of one or the other structure type depends on the relative importance of C···C and C···H interactions and therefore on the number and positioning of C and H atoms in the molecule. Consequently, it is possible to consider part of the molecular free surface as 'stack promoting' and the rest as 'glide promoting'. Individual C and H atoms in a molecule may be assigned stack and glide factors based only on their atomic connectivity. Using these factors, a predictive mapping from molecular to crystal structure is attempted. Based as they are on molecular shape, the packing criteria proposed here provide a simple classification scheme and, in some cases, may be used to predict the crystal structures of other planar aromatic hydrocarbons.

Introduction

A predictive understanding of the packing of molecular crystals has been considered increasingly important in areas as varied as solid-state chemistry, materials science and drug design. The concept of crystal engineering which describes the deliberate design of organic crystal structures for specific physical and chemical purposes has therefore elicited much interest (Schmidt, 1971; Thomas, 1974; Scheffer, 1987;

0108-7681/89/050473-10$03.00